A Data-Driven Design Framework for Wind Turbines via Design-by-Morphing and Bayesian Optimization

Hamza Latif Mehr[a], Imran Akhtar[b] and Haris Moazam Sheikh[c,*]

[a]Graduate School of Sustainable Engineering for Energy, Water and Environment (ENSE^3), Grenoble INP, Université Grenoble Alpes, Grenoble, 38000, France
[b]School of Interdisciplinary Engineering & Sciences (SINES), National University of Sciences & Technology (NUST), Islamabad, 44000, Pakistan
[c]University of Southampton, University Road, Southampton, SO17 1BJ, United Kingdom

ARTICLE INFO

Keywords:
Vertical-axis wind turbines
Shape optimization
Design-by-morphing
Hybrid blade shapes
Bayesian optimization
Computational fluid dynamics

ABSTRACT

This study presents a data-driven design optimization framework the integrates Design-by-Morphing (DbM) with Bayesian optimization (BO) to facilitate the discovery of novel, high-performance aerodynamic geometries. Applied to vertical-axis wind turbines (VAWTs), the DbM approach enables the generation of novel shapes that go beyond the conventional constraints of lift-based (Darrieus) and drag-based (Savonius) geometries. Candidate designs were evaluated via expensive high-fidelity Unsteady Reynolds-Averaged Navier-Stokes (URANS) simulations under representative urban wind conditions, with the design space systematically explored to maximize the power coefficient, C_P. From a design space of 6.28 million configurations, the BO-driven framework identified a high-performance design within a remarkably low number of iterations. The optimal configuration achieved a 21.26% increase in power extraction efficiency over existing benchmark designs, while simultaneously maintaining a stable torque profile and structural robustness across a range of Reynolds numbers. Ultimately, this research establishes the DbM-BO architecture as a scalable and computationally efficient pipeline for addressing complex aerodynamic challenges where the derivation of non-intuitive, high-performing surfaces is critical.

1. Introduction

Vertical-axis wind turbines (VAWTs) have attracted increasing interest for urban and decentralized applications because of their omnidirectional operation, ease of installation, and lower noise levels [1, 2]. Their wider adoption, however, has been limited by inherently lower aerodynamic efficiency: while horizontal-axis wind turbines (HAWTs) can reach efficiencies of 50–55%, VAWTs typically achieve only 30–40% [3]. This performance gap stems largely from the strong dependence of aerodynamic output on blade shape, turbine configuration, and tip-speed ratio (TSR). Historically, drag- and lift-based blade shapes for VAWTs were derived from engineering intuition built on decades of HAWT research, but VAWTs exhibit fundamentally different flow physics, so aerodynamically optimal design concepts do not directly translate. Therefore, systematic VAWT optimization that avoids existing designer biases is needed [4], and recent research has begun to pivot toward developing truly high-performance VAWT rotors.

To overcome the low aerodynamic efficiency associated with conventional blade geometries, recent studies have increasingly employed intuitive hybrid designs that combine lift and drag-based turbine characteristics [5, 6]. The emergence of advanced additive manufacturing techniques has enabled the realization of geometries that were previously impractical to fabricate [7], supporting research in non-intuitive designs as well. Several review studies have summarized the aerodynamic design space of VAWTs and highlighted the key parameters governing their performance. Bhutta et al. [8] provided an early comprehensive review of VAWT configurations and design methodologies, emphasizing the influence of rotor solidity, blade number, and airfoil selection on turbine efficiency. More recently, Shen et al. [9] reviewed performance enhancement strategies for Darrieus turbines and reported that improvements are typically achieved through blade-geometry refinement, flow control techniques, and optimized operational parameters. These studies collectively demonstrate that VAWT performance depends on a complex interaction between geometric and operational variables, making systematic optimization approaches particularly valuable.

In addition, several recent works have investigated specific aerodynamic parameters affecting VAWT performance. Kuang et al. [10] performed a systematic analysis of rotor solidity and demonstrated that turbine efficiency strongly depends on the balance between blade loading and aerodynamic losses. Experimental investigations by Peng et al. [11] further showed that turbulence intensity and inflow conditions can significantly alter the aerodynamic behavior of straight-bladed VAWTs. From a numerical perspective, Fazlizan et al. [12] reviewed CFD methodologies for VAWT analysis and emphasized the growing role of CFD-based optimization frameworks for exploring complex design spaces.

Other studies have investigated the aerodynamic optimization of VAWTs using various geometry modifications. Early efforts demonstrated that blade shape adaptation through morphing or deformation techniques combined with computational fluid dynamics (CFD) can significantly

*Corresponding author
h.m.sheikh@soton.ac.uk (H.M. Sheikh)
ORCID(s): 0000-0002-3154-0494 (H.M. Sheikh)

improve power output across operating conditions [13]. Subsequent work extended shape optimization to lift-based Darrieus and hybrid VAWT configurations using evolutionary and heuristic optimization approaches, improving performance by tuning rotor-level parameters such as blade shape, radius, height, and blade number [14]. More recent studies employed high-fidelity CFD to optimize multi-turbine arrangements, helical and hybrid blade designs, and coupled geometric and operational parameters, highlighting the importance of turbine spacing, relative positioning, rotation direction, and blade geometry for power enhancement [15, 16, 17]. While these approaches demonstrated notable performance gains, many of them relied on intuition-based trial-and-error methods or conventional shape parameterization [18], which limits the potential for truly optimized solutions free from pre-existing biases. Several studies have been confined to traditional blade shapes that either favor drag-based (Savonius) or lift-based (Darrieus) designs, without fully exploring the benefits of design shapes outside of these categories. A major constraint that has limited the design scope of previous efforts has been the prohibitive cost of evaluating a large design space using high-fidelity computational fluid dynamics (CFD) simulations or experiments [19].

In this paper, we address the limitations of previous efforts by introducing a systematic and cost-effective design approach to VAWT optimization. The objective of this research is to explore non-intuitive combinations of drag-based and lift-based blade shapes using a novel parameterization method, Design-by-Morphing (DbM), and to optimize them through Bayesian optimization, which is well-suited to costly black-box design spaces. Using CFD simulations validated on both lift-based and drag-based turbines, we evaluate the performance of hybrid blade configurations by computing the power coefficient C_P and assessing their efficiency improvements relative to traditional designs. Ultimately, the key objective of this work is to propose a scalable and computationally efficient data-driven framework for VAWT design using DbM and Bayesian optimization, while establishing a generalized methodology for discovering non-intuitive high-performance aerodynamic configurations across broader engineering applications.

2. Methodology

This study employs a three-component design methodology for aerodynamic shape optimization of VAWTs using the DbM framework. The approach includes (1) a morphing strategy for the turbine blade and rotor configuration for generating new hybrid VAWT geometries through smooth transformations between lift and drag-based turbines, (2) CFD simulations using the k–ϵ model with Enhanced Wall Treatment (EWT) to evaluate aerodynamic performance, and (3) optimization by utilizing multi-variable, single-objective Bayesian optimization, a specialized case of the MixMOBO algorithm by Sheikh et al. [20] to identify optimal blade designs with minimal CFD evaluations. Each component is detailed in subsequent subsections, and an overview of the methodology is provided in Figure 1.

2.1. Design Space Creation using DbM

Blade-shape parameterization is a central component of the DbM framework for VAWTs. Conventional shape parameterization techniques, such as Free-Form Deformation (FFD), PARSEC, Bézier curves, and B-splines provide flexibility for aerodynamic design but often impose geometric constraints, require a large number of control variables, and limit systematic global modifications [21, 22, 23]. As a result, these approaches tend to restrict the design space to incremental, intuition-driven modifications of existing geometries rather than enabling radical global transformations. This limitation is particularly critical in aerodynamic optimization problems, where performance is strongly dependent on the overall geometry. The DbM approach addresses these shortcomings by reducing high-dimensional geometry into a compact set of design parameters, enabling global, non-local transformations and extrapolation beyond existing designs [24].

DbM, originally introduced by Oh [24], addresses these limitations by reducing high-dimensional geometric representations into a compact set of design parameters that enable global, non-local shape transformations. Instead of directly manipulating control points or local surface parameters, DbM generates new geometries by morphing among a set of topologically compatible baseline shapes. Any two-dimensional shapes bounded by a single continuous surface are homeomorphic and can therefore be mapped onto one another through a set of discrete collocation points. This mapping establishes a one-to-one correspondence between geometries, allowing shapes to be combined smoothly within a continuous design space. A key advantage of DbM is that it allows both interpolation and extrapolation between baseline shapes. While interpolation generates intermediate geometries between existing designs, extrapolation through negative weights can produce entirely new shapes that do not directly resemble any of the original baselines. Although extrapolation may occasionally introduce nonphysical geometrical artifacts such as self-intersections, these can be detected and corrected through geometric conditioning procedures, allowing the design space to remain large without compromising geometric validity.

Initial proof-of-concept studies applied DbM to high-speed train nose optimization, achieving drag reductions of up to 13% compared to conventional designs [24]. Recently, Sheikh et al. [25] showed that DbM could reconstruct the entire UIUC airfoil database with over 99.5% accuracy using a limited number of baseline airfoils. When combined with numerical simulation and optimization algorithms, the framework enabled the discovery of novel airfoil geometries that simultaneously improved lift-to-drag ratio and stall tolerance. Despite these successes in aerodynamic shape optimization, the application of DbM to VAWT blade design remains largely unexplored.

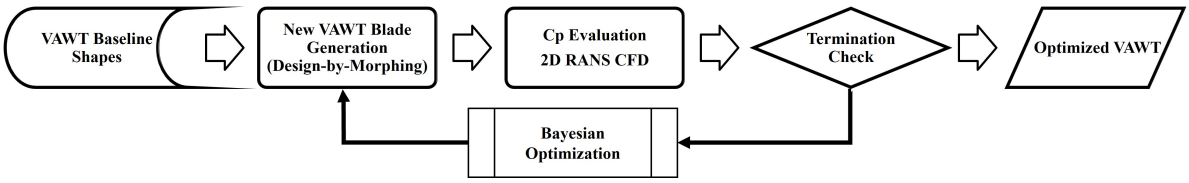

Figure 1: Overview of the methodology combining DbM, CFD, and Bayesian optimization in a loop.

In this study, DbM enables non-intuitive shape exploration by morphing between homeomorphic baseline shapes; the Darrieus NACA 0021 (lift-based) [26], Hybrid cusped Gottingen (goe) 395 airfoil [27], and Savonius (drag-based) [28] profiles as shown in Figure 2. These baselines are conventional geometries for VAWTs in the literature. Previous DbM applications have shown that this strategy can work well even with hallucinated baseline shapes since DbM can negatively weight these shapes, but such shapes can increase the infeasible regions of the design space [29, 25]. In order to keep the dimensionality of the VAWT design space reasonable and maximize the number of candidate designs, we chose existing VAWT geometries as DbM baselines.

By morphing these conventional baseline shapes, DbM creates a flexible design space beyond conventional parameterization, enabling both interpolation and extrapolation of shapes while reducing user-imposed bias. Since simulations are primarily 2D, the baseline shapes are adopted in two dimensions. These geometries must be homeomorphic, with point-to-point correspondence across all blades, ensured through a collocation procedure. Morphed designs are generated by applying weights in spherical coordinates, enabling interpolation and extrapolation of the baseline designs. The DbM design framework is based on an n-sphere formulation, as explained by Lee et al. [30]. The n-sphere equations for DbM are given as:

$$S^n = \left\{ \mathbf{x} \in \mathbb{R}^{n+1} : \|\mathbf{x}\| = R \right\}, \tag{1}$$

where R is the radius of the VAWT and generalized spherical coordinates allow mapping from Cartesian to spherical space [31]:

$$\begin{aligned} x_1 &= r\cos(\varphi_1), \\ x_2 &= r\sin(\varphi_1)\cos(\varphi_2), \\ &\vdots \\ x_n &= r\sin(\varphi_1)\cdots\sin(\varphi_{n-2})\sin(\varphi_{n-1}). \end{aligned} \tag{2}$$

For three baseline shapes ($n = 3$), morphing weights (w_1, w_2, w_3) on the n-sphere are

$$w_1 = \cos(\varphi_1), \quad w_2 = \cos(\varphi_2)\sin(\varphi_1), \quad w_3 = \sin(\varphi_2), \tag{3}$$

yielding the morphed blade as:

$$\mathbf{A}_{\text{morphed}} = w_1\mathbf{A}_1 + w_2\mathbf{A}_2 + w_3\mathbf{A}_3 \tag{4}$$

where A_1, A_2, and A_3 are the collocated baseline shapes corresponding to the drag-based, goe-395 based, and lift-based profiles. Normalization of the turbine to a radius R = 0.5 m ensures that the L2 norm is 0.5, placing all weights on the half-unit sphere and guaranteeing smooth transitions.

$$\|\mathbf{w}\|_2 = \sqrt{\sum_{i=1}^{n} w_i^2} = R \tag{5}$$

Collocation forms the basis of DbM and is applied to the VAWT baseline shapes to establish point-wise correspondence between the three blades of baseline geometries, enabling smooth morphing transformations in the DbM framework. The blade curve is parameterized by arc length and uniformly resampled. The upper part of the contour is then mirrored to form a continuous open curve for morphing. After applying the morphing weights, the new contour is mirrored back to close the curve and form the hybrid blade. Negative morphing weights can yield invalid geometries due to self or inter-blade intersections. Rather than discarding them, automated algorithms are applied to retain design diversity. More details on intersection removal are given in Appendix A.

Morphed blade geometries are generated by varying the spherical weight factors ϕ_1 and ϕ_2 within the range 1° to 179°, sampled approximately every 15°. This results in 13 discrete values for each parameter and a total of $13 \times 13 = 169$ distinct blade configurations. The endpoints were set to 1° and 179° instead of 0° and 180° to avoid reproducing the baseline shapes. The morphing loop spans drag-based and lift-based geometries, transitioning through hybrid profiles around $\phi_1 = 90°$ and $\phi_2 = 90°$, and producing a wide range of unconventional and intersected blade shapes, including non-intuitive configurations. Following blade morphing, turbine configurations were defined using three geometric parameters normalized by the unit diameter: inter-blade distance $d_x \in [0 : 0.045 : 0.45]$, vertical placement $d_y \in [0 : 0.25 : 1]$ (representing the percentage of blade above the y-axis), and blade rotation angle $\theta \in [0 : 15 : 180]°$ with symmetry at $\pm 180°$.

In addition, the operational parameter tip-speed ratio (TSR) was evaluated in the range from 0.5 to 4.5 based on previous VAWT studies [26, 28], with 13 discrete values [0.5 : 0.3333 : 4.5]. Another parameter of rotation direction was introduced in terms of positive or negative TSR, as some shapes rotate in a clockwise direction and some in an anti-clockwise direction based on the resultant force on the

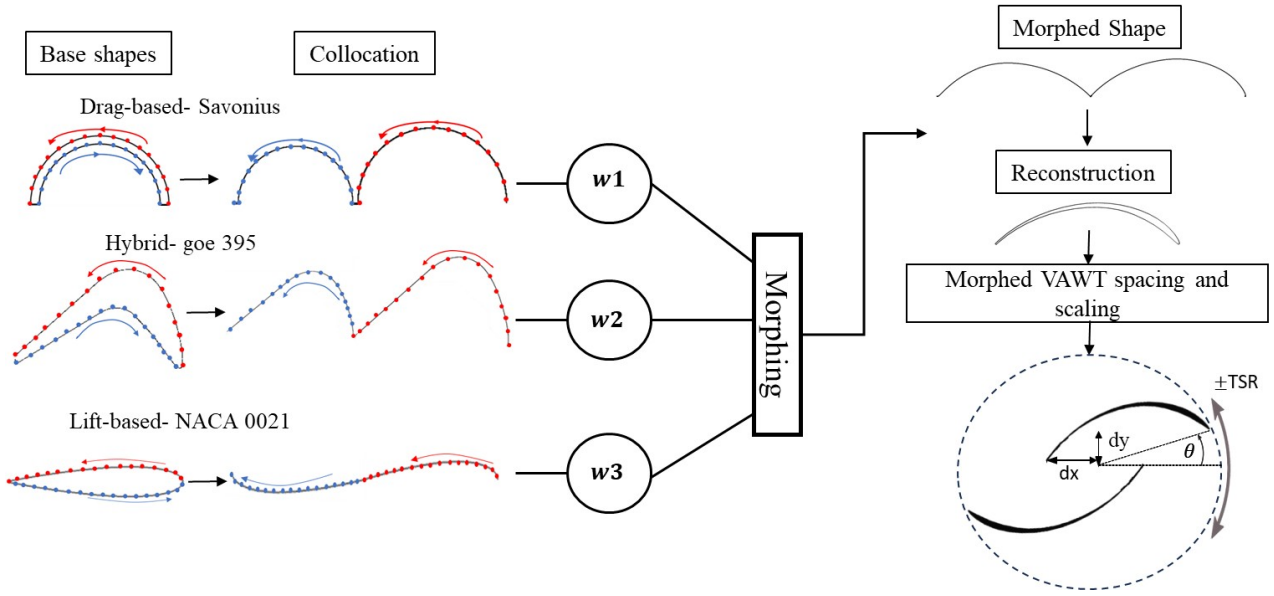

Figure 2: DbM framework for generating hybrid VAWT blade geometries. Collocated baseline blades (Savonius, goe 395, and NACA 0021) are morphed using weights (w_1, w_2, w_3) to produce new blade shapes, which are then reconstructed and positioned using geometric parameters dx, dy, blade rotation θ, and TSR in either direction for the CFD simulations

blade shape. Together, these parameters enable full coverage of the design space for all morphed blade geometries, while allowing extrapolation beyond interpolation through negative morphing weights, leading to novel hybrid lift–drag VAWT configurations. The resulting blade transformations are illustrated in Figure 2. The integrated framework couples DbM geometry generation with MixMOBO optimization. The optimizer proposes a set of discrete design variables for the VAWT design, which are used by DbM to generate a CAD-valid blade geometry. This geometry is then evaluated using CFD to compute the objective function. The process is repeated iteratively until the optimal configuration is identified. The design variables supplied to MixMOBO yield 6.28×10^6 combinations.

2.2. CFD Solver

CFD simulations have become indispensable for assessing turbine performance during shape parameterization studies, however they face inherent trade-offs between accuracy and computational cost. Conventional 2D models often overpredict efficiency by up to 32% due to neglected 3D vortex dynamics, while high-fidelity 3D simulations with LES provide more realistic predictions [32, 33]. Approaches such as RNG and realizable k–ε models [34] and the k–ω SST formulation [35] have been widely used in VAWT simulations, while hybrid RANS–LES strategies offer a compromise between accuracy and cost [36]. However, the EWT model [37] used with the k–ε model provides a more flexible alternative by smoothly bridging the viscous sublayer and log-law region through a damping function, ensuring accurate near-wall predictions without fine-tuning initialization parameters as in the k–ω SST model. This flexible formulation makes EWT particularly attractive for relatively unexplored VAWT applications. This section presents the numerical methodology used to simulate and validate VAWT performance. The objective is to develop an efficient CFD model using EWT that remains robust across a range of TSR values.

Table 1
Verification and Validation Error Summary

Verification / Validation Source	Error (%)
TURB Model 2D Drag (k-ϵ EWT vs CFD [33])	2.20
TURB Model 2D Drag (k-ϵ EWT vs k-ω)	1.00
TURB Model 3D Drag (k-ϵ EWT vs Experiment [28])	6.20
TURB Model 3D Drag (k-ϵ EWT vs k-ω)	0.33
Mesh Verification Drag	0.03
Mesh Verification Lift	0.91
Time-step verification	0.003
Validation 2D Lift vs CFD [32]	5.00
Validation 2D Lift vs Experiment [26] (Avg.)	16.70
Validation 2D Drag vs Experiment [28] (Avg.)	20.00
Validation 3D Drag vs Experiment [28] (Avg.)	6.50

The CFD verification and validation methodology was systematically adapted, beginning with model verification in a simpler static configuration, followed by mesh and time-step independence studies for rotating cases, and concluding with validation against experimental data for both drag and lift-based designs accross the complete range of TSR to ensure the accuracy and reliability of the simulations as summarized in Table 1; further details are provided in Appendix B. Overall, the CFD model using the k–ε EWT provided accuracy comparable to that of the k–ω SST model within 1% but with reduced sensitivity, hence a lower computational cost, as the optimization required a large number of unsteady CFD simulations. Then, mesh verification was performed using Richardson extrapolation for both drag- and lift-based

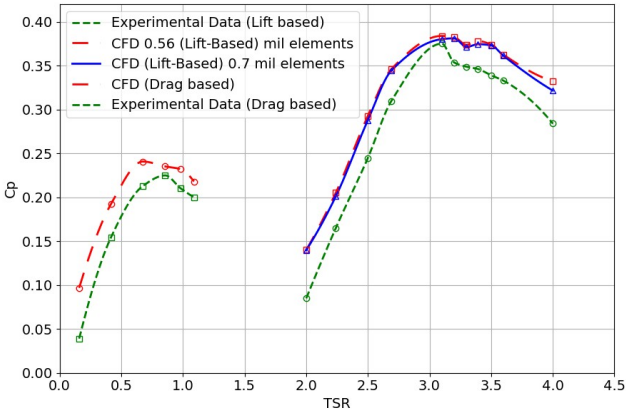

Figure 3: Validation of Savonius (Drag-based) with Blackwell et al. [28] and Darrieus (Lift-based) turbines with Bachant and Wosnik [26].

turbines, resulting in a GCI of less than 1%. Since the simulations were unsteady RANS, time-step independence was also evaluated, and a time step of 0.0025 s was selected as optimal, yielding less than 1% error across the full TSR range.

Validation against experimental studies on both lift-based and drag-based turbines confirmed its suitability for the subsequent optimization study, with an average (over TSR range) of 16% error for 2D lift-based turbines and an average of 20% error for drag-based turbines. Validation against experimental data of Bachant's NACA 0021 matched the C_P curve with $< 10\%$ error at mid-TSRs as seen in Figure 3. For drag-based turbines, simulations compared well with Blackwell's experiments, with C_P errors $< 15\%$ at most TSRs, though 2D overpredicted at very low TSR and high TSRs due to 2D simulation neglecting 3D turbulence effects. The overall trend of C_p with respect to TSR remains the same, making 2D CFD a tractable solver for optimization.

To identify the source of this error in the 2D analysis, the results were compared with 2D results reported in the literature, resulting in an average of 3% difference. However, validation of 3D CFD using the same CFD model as used in 2D before against experimental data resulted in only 6.5% error. The data are shown in Table 1. These results indicate that 2D simulations tend to overpredict separation effects, leading to relatively higher errors at lower TSR. It was observed that the 2D simulations overpredicted the C_Q, particularly at low TSR, due to the limitation of two-dimensional models in capturing turbulence and tip vortices; however, they still follow the torque trend closely. To balance computational cost and accuracy, 2D simulations were selected for the optimization process. The following section describes the multivariable optimization methodology adopted.

2.3. Bayesian Optimization

CFD simulations in VAWT optimization problems are considered to be expensive, hence a cost-effective optimization algorithm is critical. Gradient-based methods converge quickly but risk local optima, while heuristic strategies such as genetic algorithms or particle swarm optimization require many evaluations, especially for multivariable optimization [38, 39, 40, 41]. Bayesian optimization, particularly in multi-objective and mixed-variable algorithms like MixMOBO [20], offers a promising approach by using surrogate models to balance exploration and exploitation of the design space [42, 43, 44, 45]. However, integration of DbM with a sample-efficient global optimization framework remains largely unexplored for VAWT, representing a key gap. This section presents the multi-variable Bayesian optimization methodology adopted for VAWT blade design. MixMOBO is well-suited for such black-box functions as it constructs a surrogate model, typically a Gaussian process (GP), to guide the search using relatively few evaluations. The GP provides both predictions and uncertainty estimates, enabling the optimizer to balance exploration of uncertain regions and exploitation of promising designs.

The optimization follows an iterative loop: (i) initialization with a small set of CFD-evaluated points, (ii) surrogate model construction, (iii) acquisition function maximization, (iv) objective evaluation by CFD, (v) model update, and (vi) repetition until convergence. For this study, we adopt the MixMOBO strategy developed by Sheikh et al. [20], which can optimize a mixed-variable design space using very few function calls, i.e. numerical simulations. We note here that the optimization problem is not inherently mixed-variable and can be posed in continuous space. However, probabilistic global optimizers such as Bayesian optimization balance exploration and exploitation, and may devote excessive evaluations to very small 'neighborhoods' when the objective is high-frequency and/or noisy [46]. This necessitates larger budgets to globally optimize an expensive design space. By discretizing the search space and treating variables as integers, this issue is somewhat mitigated, as it prevents the algorithm from spending too much time exploring near-identical data points [30]. Compared to conventional BO algorithms, MixMOBO is efficient with mixed variables, making the optimization more sample efficient.

Before actual deployment, the MixMOBO optimization framework was validated on a set of benchmark optimization problems. Five standard test functions [47] were used (Rastrigin, Styblinski–Tang, Rosenbrock, Ackley, and Spherical), where each test function was evaluated over 10 independent runs. The design space dimensionality for these test functions was fixed to be similar to our design problem. For each run, 50 initial samples were drawn, followed by 180 iterative evaluations. The metric used for comparison is the normalized reward, which converges to 1 when the global optimum is reached. It is defined as:

$$\text{Normalized Reward} = \frac{f_{\text{current optimum}} - f_{\text{random sample optimum}}}{f_{\text{global optimum}} - f_{\text{random sample optimum}}}$$

Figure 4 shows the mean normalized reward achieved by MixMOBO across the benchmark functions, with shaded regions representing $0.5 \times$ standard deviation (for visualization). The results demonstrate that MixMOBO consistently

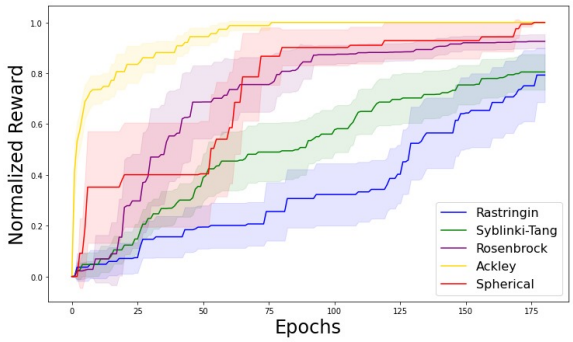

Figure 4: Validation of MixMOBO on five standard benchmark functions. Mean normalized reward is plotted with shaded regions representing 0.5× standard deviation [20].

approaches the global optimum within the prescribed budget, confirming its suitability for our expensive-to-compute black-box VAWT design problem.

2.4. Optimization Setup

The study targets small-scale turbines for urban winds, i.e., $V_\infty \approx 6$ m/s, $Re \approx 4.0 \times 10^5$ [48]. The optimization is conducted under several simplifying constraints. The rotor diameter is fixed at 1 m to provide a normalized reference scale for the design variables, as also explained in Section 2.1. A two-dimensional computational fluid dynamics model is used because it has been validated for relative performance comparisons while remaining computationally efficient for large optimization sweeps. In addition, the study is limited to two-bladed rotors to maintain geometric consistency and reduce the dimensionality of the design space. The optimization results are described in the following sections. The optimization study is performed using an integrated DbM-CFD-MixMOBO framework executed in an iterative loop with two manual checkpoints at mesh generation and post-processing. An initial batch of 50 randomly sampled designs is evaluated to map the design space and fit the GP surrogate model in the MixMOBO framework.

Among these initial evaluations, the DbM generated several non-intuitive blade geometries, highlighting the flexibility of the morphing-based parametrization. The best-performing initialization design corresponded to a hybrid blade geometry defined by $\phi_1 = 60°$ and $\phi_2 = 150°$, with configuration parameters $\theta = 165°$, $dx = 0$, and $dy = 0.75$, achieving a power coefficient of $C_P = 0.1333$ at a tip-speed ratio of 0.83. The configuration has the characteristics of airfoil-like blade characteristics morphed into a Savonius-type turbine, demonstrating the ability of DbM to uncover unconventional yet high-performing designs. This was the starting point for sequential optimization using MixMOBO. The optimization then proceeded sequentially by evaluating one BO-identified candidate design per iteration, until 180 simulations were completed. In each iteration, the MixMOBO algorithm proposed a new design point, which was converted into the corresponding blade geometry and VAWT configuration using the DbM framework. The generated geometry was then meshed and simulated using CFD, after which the resulting power coefficient (C_P) was extracted and returned to the optimizer to inform the next iteration.

3. Results

3.1. Conventional VAWT Configuration Analysis

To evaluate the effectiveness of the proposed optimization framework, two conventional VAWT configurations were selected as benchmark cases: a drag-based Savonius rotor and a lift-based Darrieus rotor. Since both geometries are included as baseline shapes in the DbM framework, they were reconstructed directly through their corresponding morphing angles. The Savonius rotor was generated using $\phi_1 = 0°$ and $\phi_2 = 0°$, while the Darrieus rotor was generated using $\phi_1 = 90°$ and $\phi_2 = 90°$. This allowed the conventional shapes to be reproduced within the same DbM design constraints used for the optimized configurations.

The Savonius benchmark adopted an overlap ratio of $s/d = 0.18$, based on Blackwell [28], where a small overlap between buckets that was $s/d = 0.20$ improves performance. The Darrieus benchmark used a two-bladed rotor with chord length $c = 0.05$ m, close to the 54 mm NACA 0021 configuration of Bachant et al. [26]. The small chord difference in lift-based and overlap difference in drag-based VAWT results from the discretized parameter step size used in the DbM design space. Both benchmarks were evaluated at $Re = 4 \times 10^5$, $D = 1m$ using the same computational domain, mesh strategy, numerical schemes, and two-bladed constraint as the optimization cases.

A complete TSR sweep from 0.5 to 4.5 was performed for both benchmarks to establish a conventional performance standard for calculating the improvement of the optimized design. As shown in Figure 8, the Savonius rotor reached its maximum $C_P = 0.2709$ at TSR = 0.83, then decreased rapidly with increasing TSR, becoming negative beyond TSR = 1.83. This confirms its suitability for low-TSR operation. The Darrieus rotor showed the opposite behavior, producing very low C_P at small TSRs, with $C_P = 0.00498$ at TSR = 0.5 and $C_P = 0.00940$ at TSR = 0.83, but increasing steadily with TSR and reaching its peak $C_P = 0.1847$ at TSR = 3.5. At the Re under consideration, the Savonius baseline outperforms the Darrieus rotor, and the drag-based baseline is used to calculate the performance improvement of the optimized designs in the subsequent sections.

3.2. Optimization Results

Using this conventional VAWT design as the reference, the DbM–MixMOBO framework was then applied to determine how far the aerodynamic performance of a VAWT could be improved through non-intuitive hybrid shape generation and optimization. Within the 180 total evaluations, the MixMOBO optimizer was able to identify several promising VAWT configurations. The optimal configuration that reached $C_P = 0.3285$ at TSR= 1.17, a 21.26% improvement over the best existing baseline at the same operating conditions (see figure 8). The optimization history with respect

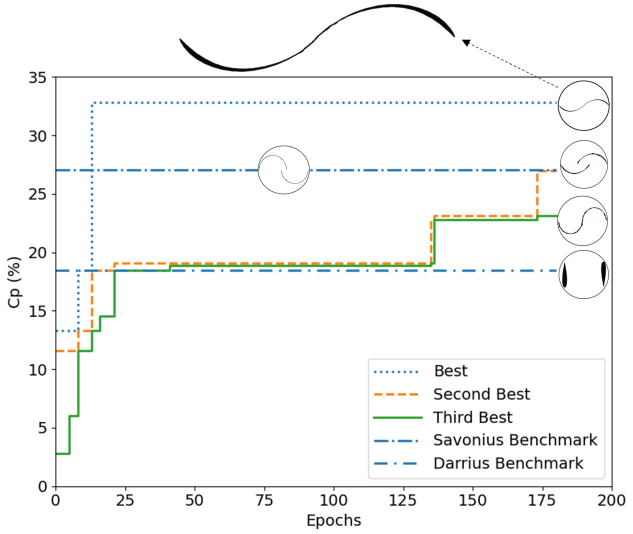

Figure 5: Comparison of power coefficient (C_P) with epochs. Darrieus benchmark is scaled for visualization.

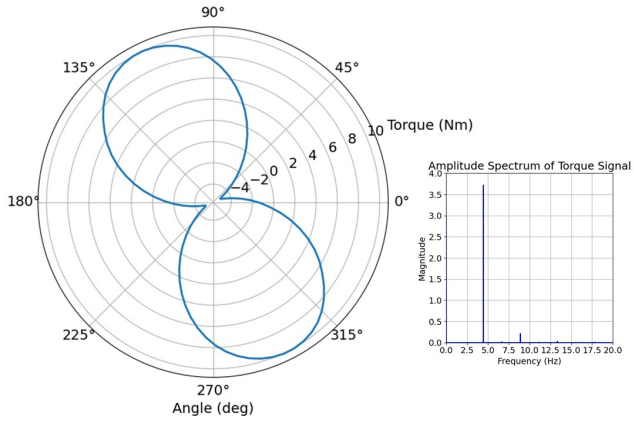

Figure 6: Torque versus azimuth and corresponding FFT for the best VAWT design

to optimizer epochs is shown in Figure 5. The majority of positive C_P designs used negative weights, highlighting DbM extrapolation; the optimizer found the improved design within 13 iterations after initialization, indicating high sample efficiency.

The optimum is an extrapolated DbM geometry resembling a high-solidity drag-based shape with contours similar to those of a lift-based shape, as shown in Figure 5. The DbM variables in this configuration are rotational direction 1 (anti-clockwise) with a blade shape rotation angle in DbM as $\theta = 180°$, blade phase angles $\phi_1 = 120°$ and $\phi_2 = 179°$, zero horizontal offset ($dx = 0$), and full vertical placement ($dy = 1$). Azimuthal torque for this best configuration in Figure 6 shows minimal torque near $\theta = 0°$, a sharp rise to 10.01 at $\theta = 115°$, followed by a decline with stall beyond $\theta \approx 135°$, with mirrored behavior from 180°–360°. The relatively smooth and periodic shape of the curve indicates stable aerodynamic behavior without abrupt dynamic stall.

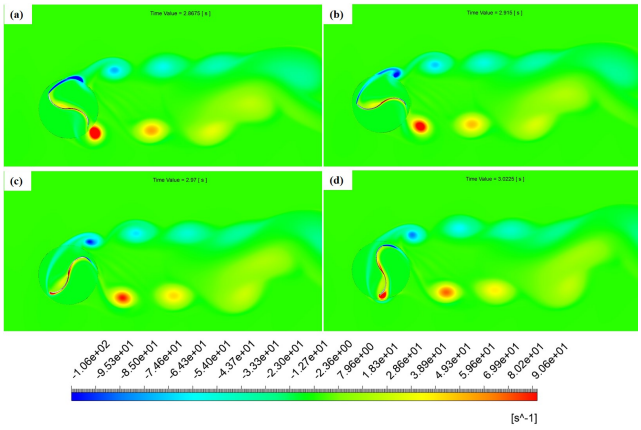

Figure 7: Vorticity contours for the optimum shape at (a) $T/8$, (b) $T/4$, (c) $3T/8$, and (d) $T/2$. Contours are symmetric from $T/2$ to T.

The vorticity contours in Figure 7 illustrate the flow mechanisms responsible for this torque variation. In frame (a), as the blade approaches $\theta \approx 90°$, a strong shear layer develops along the outer blade surface and begins to roll up into a coherent vortex. In frame (b), the vortex detaches and is convected downstream, forming the beginning of a periodic vortex street in the wake. In frame (c), the shed vortices interact with the downstream blade position, creating alternating positive and negative vorticity structures that influence the pressure distribution around the rotor. Finally, in frame (d), the vortices move further downstream, and the flow begins to reorganize around the blade and initiates a new vortex-formation cycle. This periodic vortex formation and downstream convection contribute to the stable torque response observed in Figure 6. The hybrid profile delays the performance dip to a slightly higher TSR than Savonius, consistent with added lift-based features associated with a Darrieus-type VAWT as shown in Figure 8.

To investigate the unsteady aerodynamic behavior of the optimized VAWT, a Fast Fourier Transform (FFT) was applied to the time-domain torque signal to convert it into the frequency domain as shown in Figure 6. This spectral analysis allows for the identification of dominant frequencies and potential aerodynamic instabilities that may not be evident in the time signal alone. The optimized configuration showed a clean frequency spectrum with a dominant peak at 4.44 Hz and no significant harmonics or broadband noise. This indicates a stable, periodic torque response and confirms the aerodynamic robustness of the optimized blade shape.

3.3. Comparison with Benchmarks

The optimized configuration was compared against the Savonius and Darrieus benchmark VAWT turbines under identical Reynolds number, numerical setup, and operating conditions. As shown in Figure 8, the optimum achieved a maximum $C_P = 0.3285$ at TSR = 1.17, surpassing the peak Savonius performance of $C_P = 0.2709$ at TSR = 0.83 by 21.26%, and the peak Darrieus performance of $C_P = 0.1847$

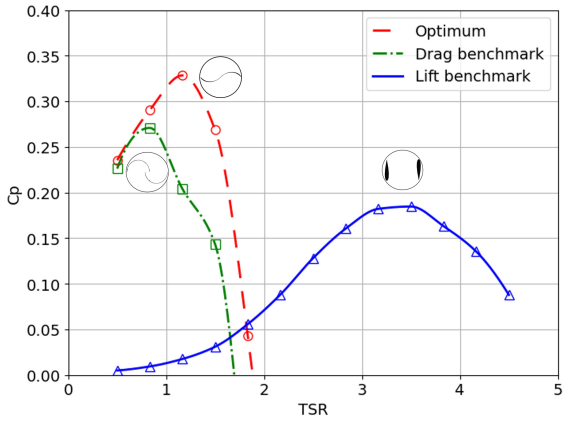

Figure 8: Comparison of benchmark drag-based (s/d = 0.2) and lift-based (scaled for visualization) configurations with optimum (Best design).

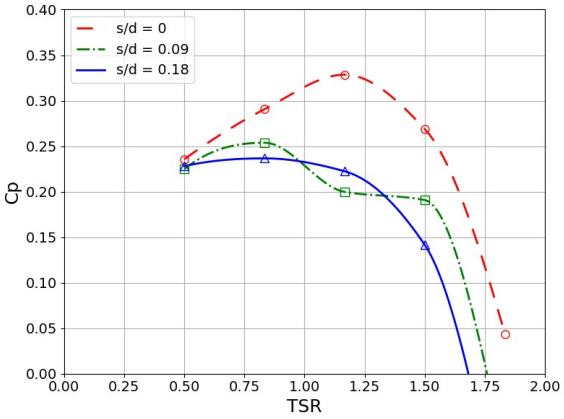

Figure 9: Comparison of overlap ratios of 0, 0.09, and 0.18 for optimum blade shape.

at TSR = 3.5 by 77.8%. At the optimum TSR, the improvement is more pronounced, with the optimized design achieving $C_P = 0.3285$ compared with $C_P = 0.2040$ for Savonius, corresponding to a 61.0% improvement. Unlike the conventional baselines, where Savonius performs efficiently only at low TSR and Darrieus becomes effective primarily at high TSR, the optimum geometry exhibits combined drag- and lift-based aerodynamic characteristics and maintains its best performance within the low-to-moderate TSR range. Since all configurations were reconstructed directly within the same DbM framework and evaluated under identical geometric and numerical constraints, the observed improvement can be attributed directly to the DbM–MixMOBO optimization methodology and its ability to identify non-intuitive hybrid VAWT configurations beyond conventional design intuition.

4. Sensitivity Analysis

The optimized design was compared with an intuitive turbine configuration to assess the impact of spacing, as conventional designs and intuition suggest that introducing a gap (s/d) can improve efficiency. To investigate this, the optimum configuration ($s/d = 0$) was compared with overlap ratios ($s/d =$, 0.09 and 0.18) to understand how the gap affects performance across various tip-speed ratios (TSRs). Additionally, the effect of Reynolds number was examined, as typical high-efficiency shapes tend to be lift-based with low solidity. However, the optimum design is drag-based shape dominant, with high solidity, making it important to assess its performance at different Reynolds numbers. Since the optimum performs best at a Reynolds number of 4×10^5, this analysis helps to determine the reason for the high solidity of the optimum shape.

4.1. Effect of Overlap (s/d) Ratio

Overlap ratios (s/d) of 0.09 and 0.18 were introduced in the optimum design to compare it with the intuitive turbine configuration. As seen in Figure 9, C_P is significantly influenced by the spacing ratio s/d across different TSRs. The optimum configuration with zero spacing ($s/d = 0$) consistently outperforms the spaced configurations across all TSR values. At TSR = 1.1667, C_P reaches its global peak of 0.3285 in the zero-spacing case, compared to 0.1998 for $s/d = 0.09$ and 0.2224 for $s/d = 0.18$, demonstrating that eliminating the gap yields the highest energy capture in the moderate TSR range. For low TSR (0.5 and 0.8333), all configurations perform relatively well, but the optimum still maintains a noticeable lead. With increasing TSR, the spaced designs deteriorate rapidly; at TSR = 1.8333 both spaced cases show negative C_P, whereas the optimum remains positive (0.0431). Overall, spacing negatively impacts performance as rotational speed increases, with $s/d = 0.18$ being the most sensitive. Thus, tighter (or zero) spacing is ideal, with the optimum performing 29.4% better than $s/d = 0.09$ and 38.8% better than $s/d = 0.18$, corroborating the efficiency of the DbM-MixMOBO approach in locating a superior configuration among millions of candidates.

4.2. Effect of Reynolds Number

It was observed that the optimization design space leaned towards low TSR at this Reynolds number and a drag-based, i.e., high solidity shape. Therefore, the influence of Reynolds number on the aerodynamic performance of the VAWT was investigated. The impact of Reynolds number on turbine efficiency was first assessed by comparing the lift-based baseline at $Re = 4 \times 10^5$ with the same turbine at $Re = 1.3 \times 10^6$. A TSR sweep for the benchmark Darrieus at both Re shows substantial gains with increasing Re, confirming that lift-based designs benefit strongly from higher Re and higher TSRs. Hence, if it were a high Reynolds number case, the optimum would lean towards a low-solidity (lift-based) design, proving the importance of Reynolds number, i.e., inlet air flow on VAWT efficiency and optimum blade shape. The detailed performance evaluation of the Darrieus turbine is given in Appendix B. Therefore, the optimized blade shape was investigated at different Reynolds numbers to analyze its effect.

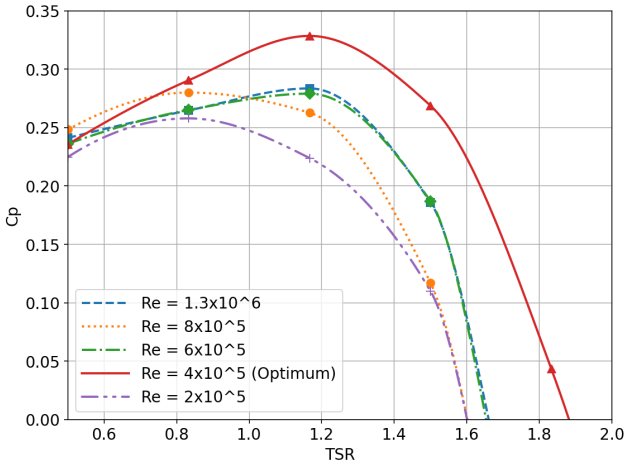

Figure 10: Comparison of C_P as a function of TSR for the optimized VAWT blade across different Re.

The optimized VAWT blade was evaluated across five Reynolds numbers (2×10^5 to 1.3×10^6) and tip-speed ratios (TSR) to assess its efficiency. As shown in Figure 10, the general trend indicates that the C_P increases with Reynolds number, reaching a peak around $Re = 4\times10^5$, followed by a slight decline or fluctuation at higher Reynolds numbers. The maximum C_P of 0.3285 is observed at $Re = 4\times10^5$ and TSR = 1.17, confirming this as the optimal operating condition for the given blade design.

Between $Re = 2\times10^5$ and $Re = 4\times10^5$, C_P improves by 46.7% at TSR = 1.17, 12.7% at TSR = 0.5, and 12.6% at TSR = 0.83. However, at higher Reynolds numbers, the performance either plateaus or declines, e.g., from $Re = 4\times10^5$ to $Re = 8\times10^5$, C_P drops by 20.0% at TSR = 1.17 and 10.5% at TSR = 1.5. At TSR = 1.83, C_P becomes negative for most Reynolds numbers, indicating reverse torque and aerodynamic inefficiency, with a value of –0.2735 at $Re = 2\times10^5$ and –0.2691 at $Re = 8\times10^5$. This drop is attributed to excessive forced rotational speeds (as the analysis has a fixed TSR as input), causing reversed flow phenomena.

The performance remains stable in the mid-TSR range (0.83–1.17) across all Reynolds numbers, highlighting the robustness of the optimized design. The non-monotonic behavior in C_P beyond $Re = 4\times10^5$ is attributed to turbulence model sensitivities, wake structure transitions, and near-wall boundary layer interactions that may not be fully captured in 2D RANS-based simulations. These results suggest that the optimized blade is best suited for moderate Reynolds number operation of $Re = 4\times10^5$, aligning with the characteristics of drag-dominant high-solidity designs.

5. Conclusion

This research presents a data-driven design framework based on a novel DbM formulation coupled with Bayesian optimization (MixMOBO), applied in the present study to improve the aerodynamic performance of VAWTs. The framework explored a high-dimensional design space composed of 6.28 million combinations and identified the optimum design within 13 iterations after initialization. This design significantly outperforms both benchmark drag-based (Savonius) and lift-based (Darrieus) turbines under similar flow conditions at $Re \approx 4\times10^5$. The benchmark sweep shows that C_P of the optimum achieved a 21.26% improvement over the C_P^{max} of Savonius and 77.85% improvement over the C_P^{max} of the Darrieus benchmark. The azimuthal torque of the optimized shape shows hybrid aerodynamic behavior, combining strong drag and lift-based characteristics, with torque rising from −4.96 at $\theta \approx 27°$ to 10.01 at $\theta \approx 115°$. FFT analysis confirms that the torque signal of the optimum is smooth and free from noise, ensuring both aerodynamic and structural stability.

Blade spacing was also analyzed, showing that the zero-spacing (optimum) case ($s/d = 0$) achieved 29.4% better C_P^{max} than 0.09 s/d and 38.8% better than 0.18 s/d. The Reynolds number sweep further highlighted that the optimum is tuned for moderate Re (4×10^5), performing 15.83% better than at $Re = 1.3\times10^6$, where lift-based designs generally dominate. These findings confirm the efficiency of the DbM and MixMOBO algorithms in generating non-intuitive high-performing turbine designs optimized for moderate Re and low TSR conditions, especially relevant for domestic and urban applications.

Overall, this study establishes a DbM and Bayesian optimization design framework for the aerodynamic design of VAWTs, enabling systematic exploration of large, non-intuitive design spaces with a limited number of parameters. The methodology demonstrates that high-performing configurations can be discovered efficiently through a coupled geometry-generation and optimization loop, without relying on conventional design intuition. Beyond the specific turbine configurations presented, the framework provides a generalizable approach to aerodynamic shape optimization problems. While the present work is based on two-dimensional CFD for computational efficiency and consistent design ranking, extending the framework to three-dimensional simulations in future work will allow the capture of additional flow physics such as tip losses, spanwise effects, and dynamic stall. Future work will also focus on experimental validation of the optimized design and the incorporation of system-level parameters, such as Reynolds number, to further assess performance under realistic operating conditions and broaden the applicability of the proposed approach.

Data availability

The data supporting the findings of this study are presented within the manuscript. Any additional data related to this work will be made available by the corresponding author upon reasonable request.

References

[1] A. Hijazi, A. ElCheikh, M. Elkhoury, Numerical investigation of the use of flexible blades for vertical axis wind turbines, Energy

Conversion and Management 299 (2024) 117867.

[2] V. Sivaram, J. O. Dabiri, D. M. Hart, The need for continued innovation in solar, wind, and energy storage, Joule 2 (2018) 1639–1642. doi:10.1016/j.joule.2018.07.025.

[3] M. Abrams, Vertical-axis wind turbines work well together, 2021. ASME. Available at: https://www.asme.org/topics-resources/content/vertical-axis-wind-turbines-work-well-together.

[4] J. R. R. A. Martins, A. Ning, Engineering Design Optimization, Cambridge University Press, 2021. Available at: https://mdobook.github.io.

[5] M. Basumatary, A. Biswas, R. Misra, Cfd study of a combined lift and drag-based novel savonius vertical axis water turbine, Journal of Marine Science and Technology 28 (2022). doi:10.1007/s00773-022-00907-4.

[6] B. P. Hand, G. Kelly, A. Cashman, Aerodynamic design and performance parameters of a lift-type vertical axis wind turbine: A comprehensive review, Renewable and Sustainable Energy Reviews 139 (2021) 110699. doi:10.1016/j.rser.2020.110699.

[7] U. Singh, M. Lohumi, H. Kumar, Additive manufacturing in wind energy systems: A review, in: Advances in Industrial and Production Engineering, Springer, 2020, pp. 757–766. doi:10.1007/978-981-15-2647-3_71.

[8] M. M. A. Bhutta, N. Hayat, A. U. Farooq, Z. Ali, S. R. Jamil, Z. Hussain, Vertical axis wind turbine – a review of various configurations and design techniques, Renewable and Sustainable Energy Reviews 16 (2012) 1926–1939. doi:https://doi.org/10.1016/j.rser.2011.12.004.

[9] Z. Shen, S. Gong, Z. Zuo, Y. Chen, W. Guo, Darrieus vertical-axis wind turbine performance enhancement approach and optimized design: A review, Ocean Engineering 311 (2024) 118965. doi:10.1016/j.oceaneng.2024.118965.

[10] X. Kuang, Z. Chen, Y. Li, X. Wang, Systematic investigation of effect of rotor solidity on vertical-axis wind turbines: Power performance and aerodynamics analysis, Journal of Wind Engineering and Industrial Aerodynamics 233 (2023). doi:10.1016/j.jweia.2022.105284.

[11] H. Y. Peng, Z. Wang, Y. Liu, J. Zhao, Optimization analysis of straight-bladed vertical axis wind turbines in turbulent environments by wind tunnel testing, Energy Conversion and Management 257 (2022) 115411. doi:10.1016/j.enconman.2022.115411.

[12] A. Fazlizan, W. K. Muzammil, N. A. Al-Khawlani, A review of computational fluid dynamics techniques and methodologies in vertical axis wind turbine development, Computer Modeling in Engineering & Sciences 144 (2025) 637–660. doi:10.32604/cmes.2025.067854.

[13] M. Baghdadi, S. Elkoush, B. Akle, M. Elkhoury, Dynamic shape optimization of a vertical-axis wind turbine via blade morphing technique, Renewable Energy 154 (2020) 239–251. doi:10.1016/j.renene.2020.03.015.

[14] Y. Chen, J. Su, Z. Han, Y. Zhao, D. Zhou, H. Yang, Y. Bao, H. Lei, A shape optimization of ϕ-shape darrieus wind turbine under a given range of inlet wind speed, Renewable Energy 159 (2020) 286–299. doi:10.1016/j.renene.2020.05.038.

[15] M. Hassanpour, L. N. Azadani, Aerodynamic optimization of the configuration of a pair of vertical axis wind turbines, Energy Conversion and Management 238 (2021) 114069. doi:10.1016/j.enconman.2021.114069.

[16] S. Sanaye, A. Farvizi, Artificial neural network and genetic algorithm for optimization of helical-blade vertical axis wind turbine, Cleaner Engineering and Technology 29 (2025) 101088. doi:10.1016/j.clet.2025.101088.

[17] M. H. Abdel-razak, M. Emam, S. Ookawara, H. Hassan, Study the performance of a novel design of twin hybrid darrieus–savonius vertical-axis wind turbines integrated with building water storage tanks: 3d optimization study, Renewable Energy 256 (2026) 124024. doi:10.1016/j.renene.2025.124024.

[18] H. Awad, E. Attia, H. Gamal, Performance and dynamic characteristics of a multi stages vertical axis wind turbine, Journal of Vibroengineering 18 (2016) 4015–4032. doi:10.21595/jve.2016.17027.

[19] S. Rasekh, S. K. Aliabadi, Toward improving the performance of a variable pitch vertical axis wind turbine (vp-vawt), part 2: Multi-objective optimization using nsga-ii with cfd in the loop, Ocean Engineering 278 (2023) 114308. doi:10.1016/j.oceaneng.2023.114308.

[20] H. M. Sheikh, Mixed-Variable Multi-Objective Bayesian Optimization, Design-by-Morphing and their Applications, Ph.D. thesis, University of California, Berkeley, 2022. Available at: https://escholarship.org/uc/item/66m2b3m9.

[21] G. Anderson, M. Aftosmis, M. Nemec, Parametric deformation of discrete geometry for aerodynamic shape design, AIAA Paper 2012–0965 965 (2012). doi:10.2514/6.2012-965.

[22] X. Han, D. W. Zingg, An adaptive geometry parametrization for aerodynamic shape optimization, Optimization and Engineering 15 (2014) 69–91. doi:10.1007/s11081-013-9213-y.

[23] D. A. Masters, N. J. Taylor, T. Rendall, C. B. Allen, D. J. Poole, Review of aerofoil parameterisation methods for aerodynamic shape optimisation, in: 53rd AIAA Aerospace Sciences Meeting, Kissimmee, Florida, AIAA 2015-0761, 2015, pp. 1–13. doi:10.2514/6.2015-0761.

[24] S. Oh, Finding the Optimal Shape of an Object Using Design-By-Morphing, Ph.D. thesis, University of California, Berkeley, 2016. Available at: https://escholarship.org/uc/item/6rd0b8rr. ProQuest ID: Oh_berkeley_0028E_16470; Merritt ID: ark:/13030/m5xw9gv4.

[25] H. M. Sheikh, S. Lee, J. Wang, P. S. Marcus, Airfoil optimization using design-by-morphing, Journal of Computational Design and Engineering 10 (2023) 1443–1459. doi:10.1093/jcde/qwad059.

[26] P. Bachant, M. Wosnik, Effects of reynolds number on the energy conversion and near-wake dynamics of a high solidity vertical-axis cross-flow turbine, Energies 9 (2016) 73.

[27] UIUC Applied Aerodynamics Group, Gottingen 395 airfoil (goe395.dat and goe395.gif), 2025. Department of Aerospace Engineering, University of Illinois at Urbana-Champaign. Available at: https://m-selig.ae.illinois.edu/ads.html, accessed April 2025.

[28] B. F. Blackwell, R. E. Sheldahl, L. V. Feltz, Wind Tunnel Performance Data for Two- and Three-Bucket Savonius Rotors, Technical Report, Sandia Laboratories, Albuquerque, NM, 1978. doi:10.2514/3.47966, issued for the United States Energy Research & Development Administration. Report No. SAN D76-0131.

[29] S. Lee, H. M. Sheikh, Airfoil optimization using design-by-morphing with minimized design-space dimensionality, Journal of Computational Design and Engineering 13 (2026) 108–124. URL: https://doi.org/10.1093/jcde/qwaf124. doi:10.1093/jcde/qwaf124.

[30] S. Lee, D. Lim, G. Gu, P. Marcus, Bayesian-optimized riblet surface design for turbulent drag reduction via design-by-morphing with large eddy simulation, Journal of Mechanical Design 146 (2024) 1–16. doi:10.1115/1.4064413.

[31] L. E. Blumenson, A derivation of n-dimensional spherical coordinates, The American Mathematical Monthly 67 (1960) 63–66. doi:10.2307/2308932.

[32] M. S. Siddique, N. Durrani, I. Akhtar, Quantification of the effects of geometric approximations on the performance of a vertical axis wind turbine, Renewable Energy 74 (2015) 661–670. doi:10.1016/j.renene.2014.08.068.

[33] E. Maican, S.-S. Biris, Comparative analysis of a wind turbine's performances by means of cfd simulations, Tarım Makinaları Bilimi Dergisi (Journal of Agricultural Machinery Science) 4 (2008) 247–252.

[34] S. A. Orszag, V. Yakhot, W. S. Flannery, F. Boysan, Renormalization group modeling and turbulence simulations, in: Near-Wall Turbulent Flows, 1993, pp. 1031–1046.

[35] F. R. Menter, Two-equation eddy-viscosity turbulence models for engineering applications, AIAA Journal 32 (1994). doi:10.2514/3.12149.

[36] O. L. J. Verhoeven, Trailing Edge Noise Simulations using IDDES in OpenFOAM, Master's thesis, Delft University of Technology, 2011. Available at: http://resolver.tudelft.nl/uuid:f382d5f3-bd63-44fe-aaf5-792e410da95f.

[37] ANSYS Inc., Enhanced wall treatment, 2009. Available at: https://www.afs.enea.it/project/neptunius/docs/fluent/html/

th/node101.htm.
[38] J. Li, M. Zhang, Data-based approach for wing shape design optimization, Aerospace Science and Technology 112 (2021) 106639. doi:10.1016/j.ast.2021.106639.
[39] B. Bastl, M. Brandner, J. Egermaier, H. Horníková, K. Michálková, E. Turnerová, Gradient-free and gradient-based methods for shape optimization of water turbine blade, in: Programs and Algorithms of Numerical Mathematics, 2019, pp. 15–26. Available at: http://eudml.org/doc/294929.
[40] D. Knight, Design optimization in computational fluid dynamicsDesign Optimization in Computational Fluid Dynamics, Springer US, Boston, MA, 2009, pp. 666–677. URL: https://doi.org/10.1007/978-0-387-74759-0_121. doi:10.1007/978-0-387-74759-0_121.
[41] D. E. Goldberg, Genetic Algorithms in Search, Optimization and Machine Learning, Addison-Wesley Longman Publishing Co., Inc., USA, 1989.
[42] Y. Morita, S. Rezaeiravesh, N. Tabatabaei, R. Vinuesa, K. Fukagata, P. Schlatter, Applying bayesian optimization with gaussian process regression to computational fluid dynamics problems, Journal of Computational Physics 449 (2022) 110788. doi:10.1016/j.jcp.2021.110788, available at: https://www.sciencedirect.com/science/article/pii/S0021999121006835.
[43] H. M. Moazam, et al., Bayesian optimization of micro-lattice defect structures using evolutionary monte carlo sampling, Science Advances 7 (2022). doi:10.1126/sciadv.abk2218.
[44] S. Gopakumar, S. Gupta, S. Rana, V. Nguyen, S. Venkatesh, Algorithmic assurance: An active approach to algorithmic testing using bayesian optimisation, in: Advances in Neural Information Processing Systems, 2018, pp. 1–9. Available at: https://proceedings.neurips.cc/paper_files/paper/2018/file/cc70903297fe1e25537ae50aea186306-Paper.pdf.
[45] D. Golovin, B. Solnik, S. Moitra, G. Kochanski, J. Karro, D. Sculley, Google vizier: A service for black-box optimization, in: Proceedings of the 23rd ACM SIGKDD International Conference on Knowledge Discovery and Data Mining, 2017, pp. 1487–1495. doi:10.1145/3097983.3098043.
[46] H. M. Sheikh, T. A. Callan, K. J. Hennessy, P. S. Marcus, Optimization of the shape of a hydrokinetic turbine's draft tube and hub assembly using design-by-morphing with bayesian optimization, Computer Methods in Applied Mechanics and Engineering 401 (2022) 115654. URL: https://www.sciencedirect.com/science/article/pii/S0045782522006090. doi:https://doi.org/10.1016/j.cma.2022.115654.
[47] Wikipedia contributors, Test functions for optimization — wikipedia, the free encyclopedia, 2025. Available at: https://en.wikipedia.org/wiki/Test_functions_for_optimization. Online; accessed 28-September-2025.
[48] S. V. Hudisteanu, C. G. Popovici, N. C. Chereches, Wind tunnel study of natural ventilation of building integrated photovoltaics double skin façade, in: E3S Web of Conferences, volume 32, 2018, p. 01020. doi:10.1051/e3sconf/20183201020.
[49] P. K. Talukdar, A. Sardar, V. Kulkarni, U. K. Saha, Parametric analysis of model savonius hydrokinetic turbines through experimental and computational investigations, Energy Conversion and Management 174 (2018) 505–518. doi:10.1016/j.enconman.2018.08.027.

Appendix

A. Intersection Removal of DbM designs

During the morphing process, certain generated blade geometries may become invalid due to intersections, which are categorized as (1) self-intersections where a blade overlaps itself due to excessive curvature or distortion, and (2) inter-blade intersections where one blade intrudes into another in a two-bladed configuration. Rather than discarding such cases, which would reduce design diversity, a set of Python-based algorithms and CAD correction techniques was developed to automatically detect and resolve these intersections.

Self-intersecting blade geometries generated during morphing were identified and corrected using geometric intersection detection, followed by reordering of coordinate points between intersection locations to restore a continuous contour. Local stiffening was applied by removing closely spaced points near intersections and interpolating between remaining coordinates to eliminate sharp curvature, with the process repeated until all self-intersections were resolved. For more complex cases involving multiple independent intersections, each blade segment was corrected sequentially before addressing cross-segment overlaps. In multi-bladed configurations, inter-blade overlaps were handled through geometric reconstruction in CAD that preserves the outer envelope of the intersecting blades, yielding a unified, physically feasible geometry suitable for meshing, CFD simulation, and subsequent analysis.

B. Computational Fluid Dynamics Simulation Setup

ANSYS Fluent was used for CFD analysis, where a sliding mesh approach was employed, with a rotating inner domain of $1.2D$ inside a stationary outer domain. Domains extended $10D$ downstream and $3D$ upstream, with $6D$ lateral spacing to minimize blockage as shown in Figure 12. The domain for 3D CFD analysis is shown in (a), high-fidelity Savonius cases included end plates of thickness $1.1D$ [49], 2D Savonius geometry at (b), 2D Darrieus geometry following Bachant et al [26] at (c), and finally 2D Darrieus geometry following Siddique et al. [32] at (d). The outer domain is the same, whereas the difference is only in the blade shape and the inner domain. Inlet velocity and pressure outlet boundaries were applied. Due to the rotational motion of the turbine and the continuously changing relative velocity around the blades, the local Reynolds number varies throughout the rotation. To maintain consistency and comparability across simulations, an average Reynolds number is used, calculated based on the inlet velocity and the turbine diameter.

For all Savonius-type cases, the Reynolds number is approximately 4.32×10^5 [28]. In the lift-based Darrieus validation case by Siddique et al [32], the Reynolds number is also 4×10^5. However, for the cases based on Peter Bachant's configurations, the Reynolds number is significantly higher, around 1.1×10^6 [26]. Validation and verification cases included Savonius [28, 33] and Darrieus turbines [32, 26]. Table 2 summarizes all verification and validation cases performed for both drag-based (Savonius) and lift-based (Darrieus) VAWTs. Each case targets a specific aspect of model fidelity, including turbulence modeling, mesh independence, timestep sensitivity, and comparison with CFD and experimental data (validation). Their CAD domains are shown in Figure 12 and their schematics are shown in Figure 13.

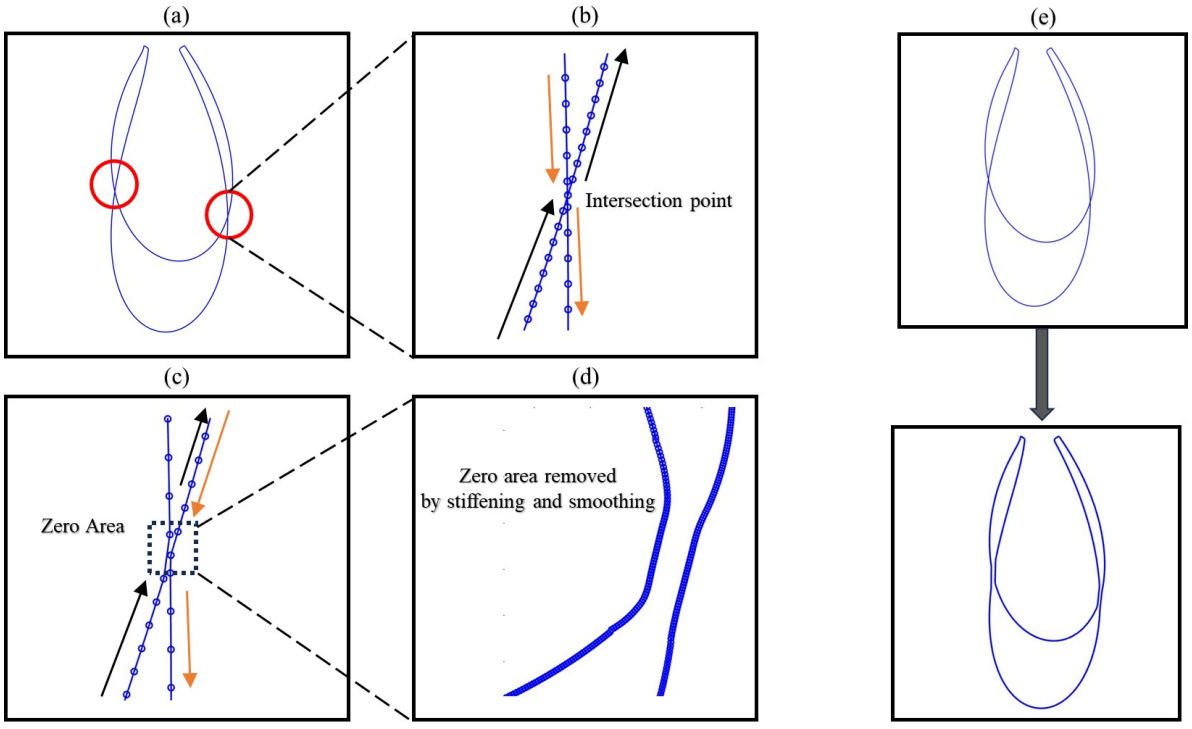

Figure 11: Intersection removal process in the DbM framework. (a) Detection of self-intersection regions in the morphed blade geometry (highlighted). (b) Local view of the intersection point showing coordinate directions. (c) Removal of the zero-area region by flipping the intersecting coordinate segment. (d) Stiffening and smoothing of the corrected contour to restore geometric continuity. (e) Transformation from intersecting blade geometry to final non-intersecting blade geometry after correction

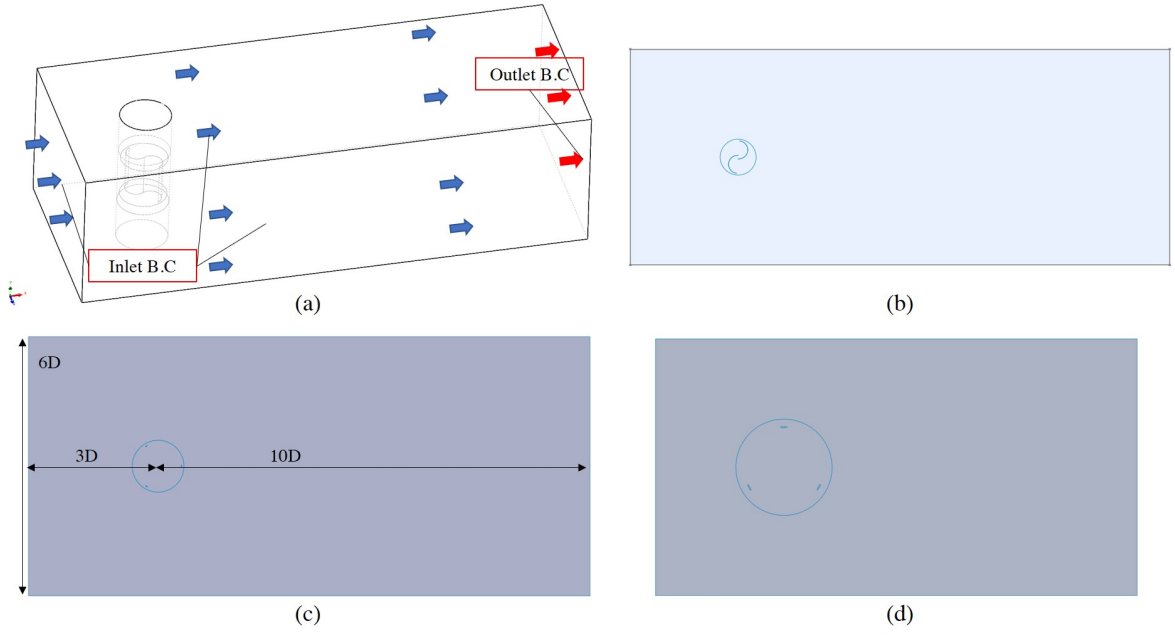

Figure 12: Domain for (a) Case 2 & 4, (b) Case 1 & 3, (c) Case 6, and (d) Case 5.

Definition of VAWT parameters. The spacing ratio s/d represents the overlap ratio, defined as the distance between blade centers (s) normalized by rotor diameter (d). A value of $s/d = 0$ indicates no overlap, while $s/d = 0.2$ corresponds to a 20% normalized spacing between blades. The angle $\alpha = 5°$ denotes a static blade angle of attack used only for model verification in non-rotating conditions. Static cases isolate aerodynamic loading without rotational effects,

Table 2
Verification and Validation cases for Savonius and Darrieus VAWTs

Type of VAWT	Case #	Validation case type	Validation parameter w.r.t. C_Q & C_P	Case parameter
Savonius Two-bucket (Drag Type) VAWT	1	2D Static, Maican [33]	5° α, s/d = 0.2, TSR = 0.1586	Model Verification
	2	3D Static, Blackwell (Run 12) [28]	5° α, s/d = 0, TSR = 0.1586	Model Verification
	3	2D Dynamic, Blackwell (Run 37) [28]	Multiple TSR, s/d = 0.2	(i) Timestep Verification (ii) Mesh Verification (iii) Validation with Experiment
	4	3D Dynamic, Blackwell (Run 37) [28]	Multiple TSR, s/d = 0.2	Validation with Experiment
Darrieus (Lift Type) VAWT	5	2D NACA 0022 Dynamic, Siddique et al. [32]	TSR = 3.0	Validation with CFD
	6	2D NACA 0021 Dynamic, Peter Bachant [26]	Multiple TSR	(i) Mesh Verification (ii) Validation with Experiment

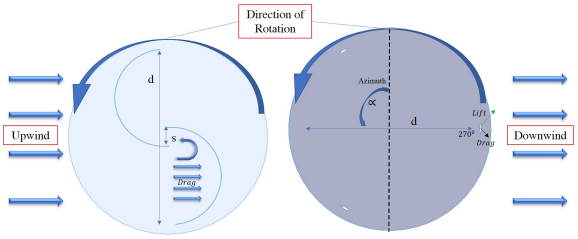

Figure 13: Schematic for (a) Savonius and (b) Darrieus turbines

allowing turbulence model validation. TSR is defined as $\lambda = \omega R/V_\infty$, governing dynamic turbine operation.

Case 1 – 2D Static (Maican). A two-dimensional static simulation at $\alpha = 5°$, $s/d = 0.2$, and TSR = 0.1586 was conducted for turbulence model verification against literature CFD. This case validates the EWT implementation under controlled, non-rotating conditions.

Case 2 – 3D Static (Blackwell, Run 12). A three-dimensional static validation at $\alpha = 5°$ and $s/d = 0$ compares simulated torque with experimental data. This builds confidence in the 3D EWT model before dynamic simulations.

Case 3 – 2D Dynamic (Blackwell, Run 37). Dynamic simulations at multiple TSR values with $s/d = 0.2$ are used for timestep verification, mesh independence assessment, and experimental validation. This case ensures temporal and spatial convergence of the rotating solver.

Case 4 – 3D Dynamic (Blackwell, Run 37). A full 3D rotating simulation at multiple TSR values validates the dynamic torque against experiment, confirming improved wake resolution and reduced separation overprediction relative to 2D.

Case 5 – 2D Dynamic NACA 0022 (Siddique et al.). A lift-based validation at TSR = 3.0 compares blade and overall torque with CFD literature results. This verifies aerodynamic lift prediction for rotating airfoil-based turbines.

Case 6 – 2D Dynamic NACA 0021 (Bachant et al.). Validation across multiple TSR values compares predicted C_P with experimental data at high Reynolds number. This case includes mesh verification and confirms the solver's ability to capture lift-dominant turbine behavior.

Simulations are primarily two-dimensional, incompressible URANS, with selected three-dimensional cases for validation, solved using the Finite Volume Method. Turbulence is modeled using the standard k–ε with EWT, which resolves near-wall regions without strict y^+ constraints ($y^+ = 1$) under y^+ <5. The two transport equations are supplemented by EWT blending functions [37]. For comparison, the k–ω SST model [35] was also applied, though it requires fine-tuning of initialization parameters and a higher mesh sensitivity for each TSR and Re. Numerical solutions used the SIMPLE algorithm with second-order schemes and convergence criteria of 10^{-5}.

B.1. Independence Studies

First model independence (Case #1) was tested using both k–ω SST and k–ε EWT. Simulations were compared with static (non-rotating) VAWT torque data. In 2D static validation (Maican [33]), C_Q showed < 3% error, confirming EWT suitability. A 3D static case (Case#2) yielded < 7% deviation from experiment, which was comparable with k–ω SST with only an absolute difference of 0.3%.

Mesh independence (Case #3 and 6) was achieved at ∼0.55M elements for both Savonius and Darrieus as shown in Figure 14. To rigorously assess mesh convergence, Richardson extrapolation was performed for the torque coefficient (C_Q) at TSR = 0.1586 using three systematically refined meshes (0.41M, 0.55M, and 0.87M elements) for the Savonius Turbine. The extrapolated solution was found to be $C_Q^{\text{ext}} \approx 0.61004$, with a grid convergence index (GCI) of

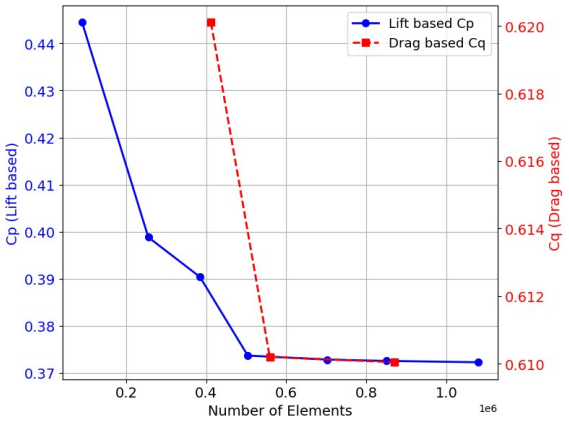

Figure 14: Mesh independence for Savonius (Drag-based) and Darrieus (Lift-based) turbines

Table 3
Timestep sensitivity analysis for C_Q at TSR = 0.1586

Timestep (s)	CFD (Present)	Percentage Error (%)
0.01	0.61005	–
0.005	0.6102	0.0246
0.0025	0.61022	0.0033

approximately 0.03% between the medium and fine meshes. These results confirm that the medium mesh (0.55 million elements) provides sufficient accuracy for the present simulations, offering a good balance between computational cost and solution fidelity, while timestep independence (Case #3) at 0.1586 TSR converged at $\Delta t = 0.005$ s for lower TSRs, and for higher TSRs it was found to be 0.0025 s. Hence, 0.0025 s was chosen for the timestep (Table 3). Following CFD model verification, CFD validation against experimental data was conducted.

B.2. CFD validation

Validation was performed for both Drag-based and Lift-based turbines across the range of TSRs. Two validation cases were performed for lift-based turbines. First, simulations were validated with CFD of Siddique et al. [32] (Case #5) within 5% torque error as seen in Figure 15. Then, validation against experimental data of Bachant's NACA 0021 (Case #6) that matched the C_P curve with $< 10\%$ error at mid-TSRs and for drag-based turbines, Savonius simulations that also compared well with Blackwell's experiments, with C_Q errors $< 15\%$ at most TSRs as seen in section 2.2. To prove robustness of the model and the identification of overprediction of torque, a 3D Savonius (Case # 4) was analyzed with 36 million cells, which reduced error to below 9% (Table 4), confirming the robustness of the EWT approach and the limitations of 2D analysis.

B.3. Study on Darrieus turbine at variable Reynolds number

The impact of Reynolds number on the benchmark Darrieus turbine was examined by comparing performance at the

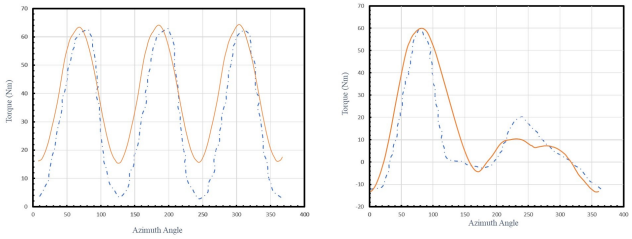

Figure 15: Overall (left) and blade torque (right) comparison with respect to azimuth angle for the present CFD results (solid line) and CFD results from Siddique et al. [32] (dashed line).

Table 4
Comparison of C_Q from 3D simulations with Blackwell [28] at TSR = 0.1586 and 0.4173.

TSR	C_Q Exp.	C_Q CFD (Present)	Error (%)
0.1586	0.382	0.365	4.4
0.4173	0.373842	0.3414	8.6

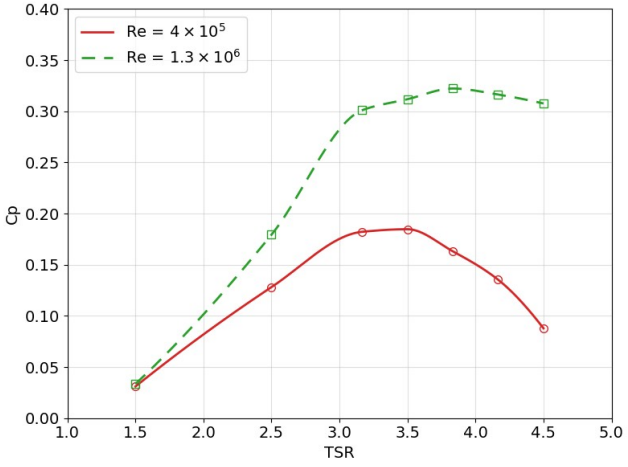

Figure 16: Comparison of Reynolds number for the benchmark Darrieus turbine at $Re = 4 \times 10^5$ (circles with solid line) and $Re = 1.3 \times 10^6$ (squares with dashed line).

baseline condition of $Re = 4 \times 10^5$ with a higher Reynolds number of $Re = 1.3 \times 10^6$. At $Re = 4 \times 10^5$, the turbine achieved a peak C_P of 0.1847 at TSR = 3.5, which is considerably lower than the performance reported by Bachant et al. [26] under higher Reynolds number conditions. To systematically assess this discrepancy, a TSR sweep was conducted at both Reynolds numbers. The results show a pronounced improvement in performance with increasing Re, particularly in the high TSR regime, where the peak C_P increases from 0.1847 to 0.3223, corresponding to a 74.5% rise. This confirms the established trend that lift-based, low-solidity turbines benefit significantly from higher Reynolds numbers due to enhanced aerodynamic lift and delayed separation. In contrast, the DbM-optimized configuration, which exhibits high-solidity and drag-dominant characteristics, is tuned for moderate Reynolds number operation around $Re = 4 \times 10^5$, where such geometries demonstrate superior performance at lower TSRs.